atoms

Tracked for Impact Factor

CITESCORE 2.8

Article

Proposal of a New Double-Nozzle Technique for In-Gas-Jet Laser Resonance Ionization Spectroscopy

Victor Varentsov

MDPI

https://doi.org/10.3390/atoms11060088

atoms

MDPI

Article

Proposal of a New Double-Nozzle Technique for In-Gas-Jet Laser Resonance Ionization Spectroscopy

Victor Varentsov

Facility for Antiproton and Ion Research in Europe (FAIR), Planckstraße 1, 64291 Darmstadt, Germany; victor.varentsov@fair-center.eu; Tel.: +49-6159711638

Abstract: This paper proposes a new double-nozzle technique for in-gas-jet laser resonance ionization spectroscopy. We explored the functionality of this new technique through detailed gas dynamic and Monte Carlo atom-trajectory simulations, in which results are presented and discussed. The results of similar computer simulations for JetRIS setup (as a typical representative of the conventional in-gas-jet technique nowadays) are also presented and discussed. The direct comparison of calculation results for the proposed new technique with the conventional one shows that the double-nozzle technique has many advantages compared with the one used in the JetRIS setup at GSI for future high-resolution laser spectroscopic study of heaviest elements. To fully implement the proposed new technique in all existing (or under construction) setups for in-gas-jet laser resonance ionization spectroscopy, it will be enough to replace the used supersonic nozzle with the miniature double-nozzle device described in the paper.

Keywords: radioactive atomic beams; gas stopping cell; supersonic gas jet; in-gas-jet laser resonance ionization spectroscopy; double-nozzle technique; gas dynamic and Monte Carlo simulations

Citation: Varentsov, V. Proposal of a New Double-Nozzle Technique for In-Gas-Jet Laser Resonance Ionization Spectroscopy. *Atoms* **2023**, *11*, 88. https://doi.org/10.3390/atoms11060088

Academic Editor: Chengjian Lin

Received: 12 April 2023
Revised: 23 May 2023
Accepted: 26 May 2023
Published: 28 May 2023

1. Introduction

For the studies of nuclear, atomic and chemical properties of radioactive elements, different techniques using gas-stopping cells are conventionally used. The primary energetic radioactive ions are injected into a gas cell filled with the high-purity buffer gas (usually helium or argon) by passing through a thin entrance window. Due to a number of their collisions with buffer gas atoms, ions decelerate down to the gas flow velocity and are thermalized. To speed up the transport of ions through big-sized gas cells, a DC gradient electric field is applied. In this case, the ion velocity is determined as a product of the applied electric field in [volt cm^{-1}] and the ion mobility coefficient in [cm^2 sec^{-1} $volt^{-1}$].

Near the extraction nozzle with a small throat diameter, ions are extracted from the gas cell into vacuum conditions by a supersonic buffer gas jet. Description of various gas cell apparatus readers can find elsewhere, for example, in [1–19] and links within them.

The extraction of the ions into a high vacuum is finally performed with the use of radiofrequency quadrupoles (RFQ) [7,8,11,20–26] or radio-frequency sextupoles (SPIG) [9,15] installed downstream for the ion beam transportation and focusing. Instead of traditional RFQ and SPIG rod structures, simple, compact, and effective gas dynamic RF-only funnels can also be used. The review of the RF-only funnel technique can find in our recent work [27].

The other way to investigate the nuclear and atomic properties of radioactive elements extracted from the gas cell is by using laser spectroscopy techniques. One can read about, e.g., recent reviews [28,29] and presentation reviews of Piet Van Duppen [30].

The most attractive and promising method of laser spectroscopy for studying the properties of radioactive elements is the so-called method of in-gas-jet laser resonance ionization spectroscopy that was first proposed and experimentally tested in KU Leuven [31]. Briefly, it consists of the following. Under the applied DC electric field gradient, the thermalized in

the high purity argon ions are transported through the gas cell and focused on the tip of the metallic hot filament. The tip of the filament has been installed on the axis of the exit flow channel in front of the nozzle. After collecting ions on the filament and their thermal evaporation as neutral atoms, they are transported by only the carrier gas flow through the converging-diverging nozzle into the vacuum gas-jet chamber. Two lasers in cross-beam geometry perform the high-resolution and efficient resonance excitation and ionization of the extracted into the gas-jet chamber neutral atomic beam. One laser beam (we will refer to as a Laser-1) directed along the axis upstream of the gas flow direction excites atoms of interest, and the second one (we will refer to as Laser-2) directed perpendicular to the gas jet ionizes these excited atoms. Then the ionized by the Laser-2 atoms are transported as the ion beam by the carrier gas jet to the bent RFQ (e.g., S-shaped [31] or bend 90 degrees [32]). This curved RFQ allows for the axial laser beam injection into the gas jet and differential vacuum pumping. One can find the schematics and descriptions of various setups for the in-gas-jet laser resonance ionization spectroscopy, e.g., in Refs. [29–38].

The article has two following goals.

The first goal—is a detailed quantitative study of the atomic beam extraction from the gas-stopping cell and then its formation and cooling in the supersonic argon gas jet under the described above traditional approach to the in-gas-jet resonance ionization laser spectroscopy. As a typical representative for this study, we have chosen the experimental gas-jet apparatus [32,33] recently created for high-resolution laser spectroscopy of the heaviest elements at the Separator for Heavy Ion Reaction Products (SHIP) at GSI, Darmstadt. This project, called JetRIS, is under development at GSI.

The second goal—is the proposal and detailed exploration of a new double-nozzle technique for its application in gas-jet resonance ionization laser spectroscopy.

We have reached both goals through computer experiments, which consisted of detailed gas dynamic and atom-trajectory Monte Carlo simulations, which results in we present and discuss below in the next sections. First, in the dynamic gas simulations of the buffer gas flow inside the gas cell and the supersonic argon carrier gas jet, we used the VARJET code. This code is based on the solution of a full system of time-dependent Navier–Stokes equations and is described in detail in [39]. The results of the gas dynamic simulations (flow fields of the buffer gas velocity, density, and temperature) we then used in atom-trajectory Monte Carlo simulations.

Similar computer simulations were also made earlier for different ion beams cooling and bunching in helium buffer gas flows, and their results are presented elsewhere (e.g., see [17–19,40–48]). Note that our calculation results (gas dynamic + Monte Carlo) for ions extracted from the gas jet into a vacuum are in good agreement with the measurements (see, e.g., [43,44]). Based on our gas dynamic calculations, setups of gas-jet internal targets [49,50] have been created. These calculations are in good agreement with the measured parameters and structure of the supersonic gas jets, as well.

For simplicity, in comparison of the two mentioned above in-gas-jet techniques, the conventional one, which is used in the project JetRIS, we will refer below to as a "GSI nozzle" and the proposed here new technique as a "double-nozzle".

2. Results for GSI Nozzle

Schematic views of the JetRIS setup are presented in both [32,33] articles.

Three different nozzles, which cross-sectional profiles are shown in [33] (see Figure 3 there), were used at the JetRIS setup in offline test measurements of neutral ^{164}Dy atoms fluorescence induced by one-step laser excitation. All these nozzles have the same throat diameter of 1 mm but different lengths and contours of diverging supersonic parts. The authors of [33] note that these three nozzles were designed for different stagnation pressure in the gas cell (P_{cell}) and background pressure (P_{bg}) in the vacuum chamber of the gas jet expansion, which we will refer to as a gas-jet chamber. The sophisticated contours of the left and right nozzles, shown in Figure 3 of Ref. [33], were designed (Ref. [35]) and produced in KU Leuven, but due to the lack of exact information available to us about

these nozzle's profiles, we could not use these two nozzles in our gas dynamic simulations. Contrary, the third nozzle, which shown in the middle of Figure 3 of Ref. [33], and referred to as the "mid-range nozzle", has a simple conical diverging part with a length of 20 mm, throat diameter of 1 mm and exit diameter of 6.6 mm.

The authors of the work [33] note, "The mid-range nozzle seems to be the best overall choice since its resolution and homogeneity are both close to the optimal values found for the other two nozzles". This is an additional reason why we chose this particular nozzle for a detailed computer study of the operation of the JetRIS setup.

The gas dynamic simulation we have performed for the argon stagnation pressure in the gas cell P_{cell} = 100 mbar and background pressure in the vacuum gas-jet chamber is $P_{bg} = 6.47 \times 10^{-3}$ mbar. The same pressure values were in the JetRIS setup during test fluorescent measurements of neutral ^{164}Dy atoms inside the supersonic argon jet (see Table 1 and the Figure 4 caption in [33]).

2.1. The Exit Flow Channel

The JetRIS gas cell technical drawing is shown in the left part of Figure 5 in [32]. The inner diameter of the gas cell DC-cage is 160 mm, with a length of 164.5 mm. The total length of the DC funnel (five electrodes having gradually decreasing diameters) placed behind the DC cage is 63.5 mm. The exit flow channel between the DC funnel and the nozzle has a diameter of 12 mm and a length of 34.6 mm. Due to the large diameter of the DC-cage (160 mm) and only 1 mm of the nozzle throat diameter, the average velocity of the gas flow inside the DC-cage is only about 8 mm/s. That is why it is necessary to use the DC gradient field inside the cell to speed up the transport of the decelerated radioactive ions.

Early, we were making detailed (gas dynamic + Monte Carlo) simulations for different big-sized gas-stopping cells [6,17–19]. E.g., the results of our simulations for the UNICELL project [51], which is also under development at GSI, presented in [17]. But here, we should notice that simulations of the ^{164}Dy ions transport through the main body of the JetRIS gas cell having an inner diameter of 160 mm to the hot filament installed inside the exit flow channel have been carefully done by the authors of [32]. Therefore, it does not make much sense to repeat it, and we decided to start our gas dynamic simulation from the entrance to this exit flow channel (12 mm in diameter), where the average gas velocity is a factor of 178 higher than it is inside the DC-cage region. Notice that the evaporated from the surface of hot filament neutral atoms are moving through the exit flow channel and then through the nozzle into the vacuum gas-jet chamber only under the effect of the gas flow.

Monte Carlo atom-trajectory simulations began from the filament tip, where neutral ^{164}Dy atoms first appear in the gas flow after evaporation. From the technical drawing presented in [32] we determined that the filament in the JetRIS setup has been installed at about 22.5 mm from the nozzle.

Results of the gas dynamic simulation for the gas velocity flow field inside the exit flow channel are shown in Figure 1.

Figure 2 shows the radial gas velocity profile in the middle of this exit flow channel. The parabolic gas velocity profile, typical for the laminar viscous gas flow inside a tube, is visible. The corresponding Reynolds number is equal to 123.

Calculation results for the time-of-flight distribution ^{164}Dy atoms from the filament tip to the nozzle throat are shown in Figure 3. The average atoms' extraction time is T = 7.0 ms, and the time spread determined as the full width at half maximum (FWHM) is ΔT = 1.4 ms. The corresponding extraction efficiency of ^{164}Dy atoms from the exit flow channel is 94.5 $\pm$ 2.7%.

2.2. GSI Nozzle at Gas Cell Pressure P_{cell} = 100 mbar and $P_{bg} = 6.47 \times 10^{-2}$ mbar

Results of the gas dynamic simulation for argon gas density, temperature, velocity, and Mach number flow fields for the GSI **nozzle** are shown in Figure 4.

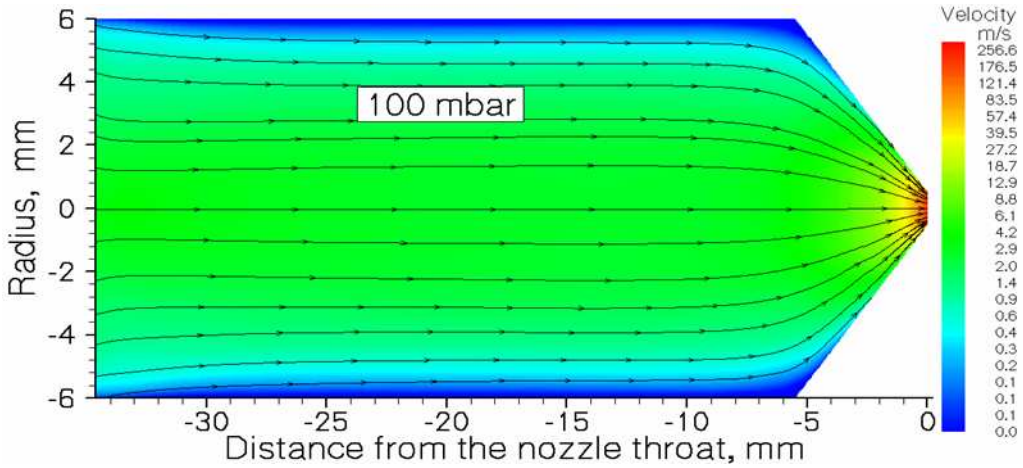

Figure 1. Results of the gas dynamic simulation for the argon velocity flow field inside the exit flow channel. The stagnation pressure Pcell = 100 mbar, and the temperature of the channel walls Tcell = 296 K. The arrowed black lines show the gas flow direction.

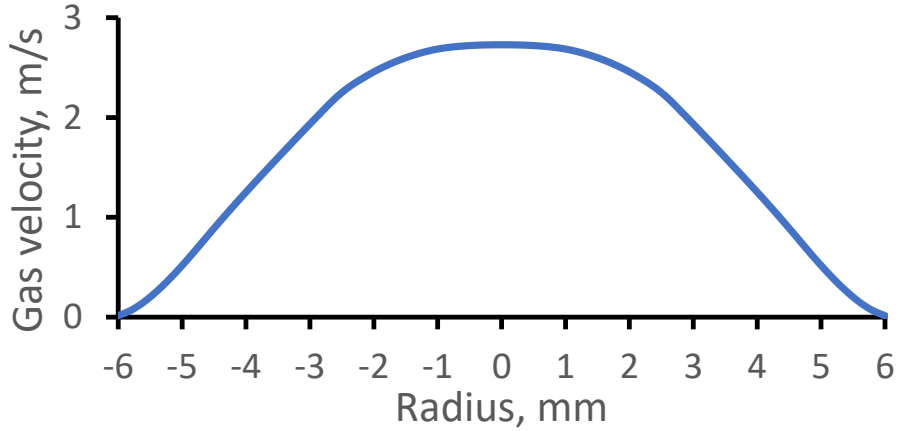

Figure 2. The calculated radial gas velocity profile is in the middle of the exit flow channel.

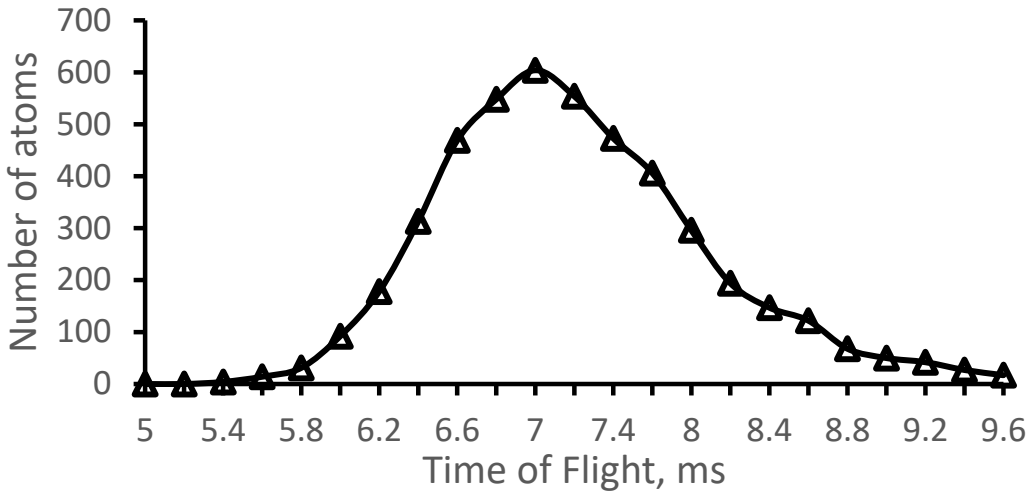

Figure 3. The time-of-flight of ^{164}Dy atoms from the filament tip to the nozzle throat. Total number of calculated atoms is 5000.

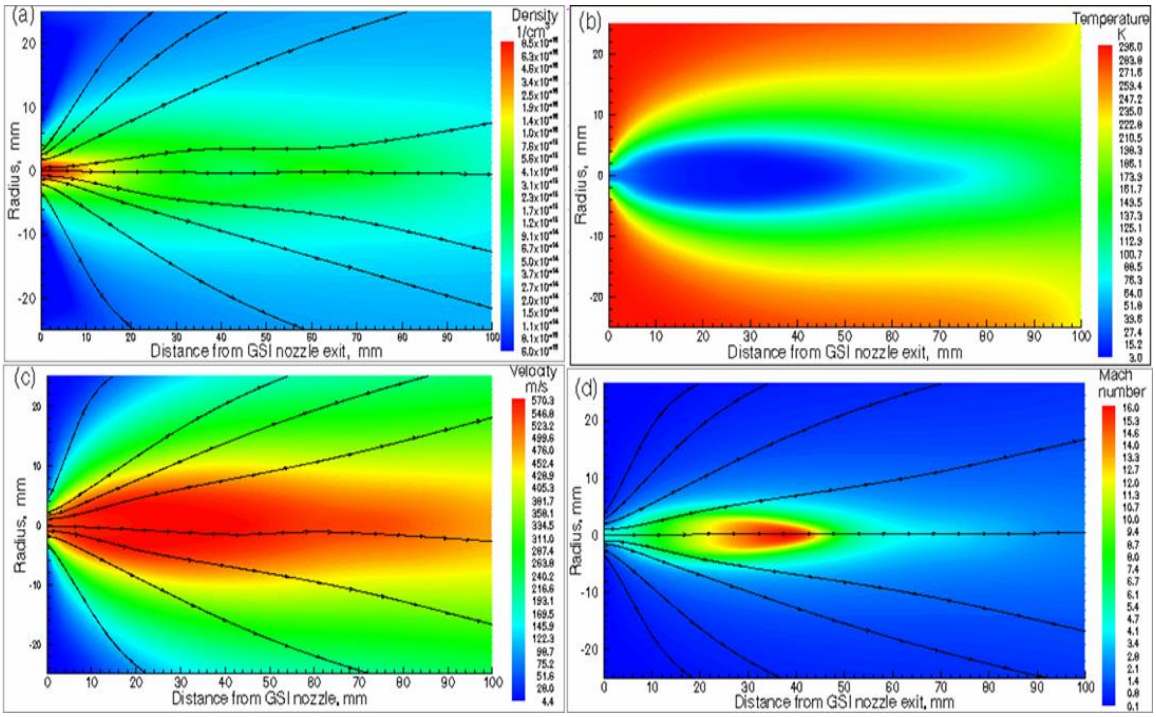

Figure 4. Results of the gas dynamic simulation for GSI nozzle: (**a**) density, (**b**) temperature, (**c**) velocity and (**d**) Mach number flow fields. The stagnation pressure and temperature in the gas cell are P_{cell} = 100 mbar and T_{cell} = 296 K, correspondingly. Background pressure in the vacuum gas-jet chamber is $P_{bg} = 6.47 \times 10^{-3}$ mbar. Black arrowed lines show the gas flow directions.

We have used the results of the gas dynamic simulation shown in Figure 4 for Monte Carlo simulations of the ^{164}Dy atomic beam. These results are presented in the next four Figures. The calculated fraction of the extracted from the gas cell ^{164}Dy atomic beam inside the region of 10 mm (the Laser-1 diameter in [33]) as a function of distance from the GSI nozzle exit is shown in Figure 5. The decrease of the dysprosium atomic beam fraction with the distance from the GSI nozzle is simply explained by the gas jet divergence. The atomic beam diffusion losses inside the GSI nozzle are equal to 15.6 $\pm$ 0.6% and are considered in the data presented in Figure 5.

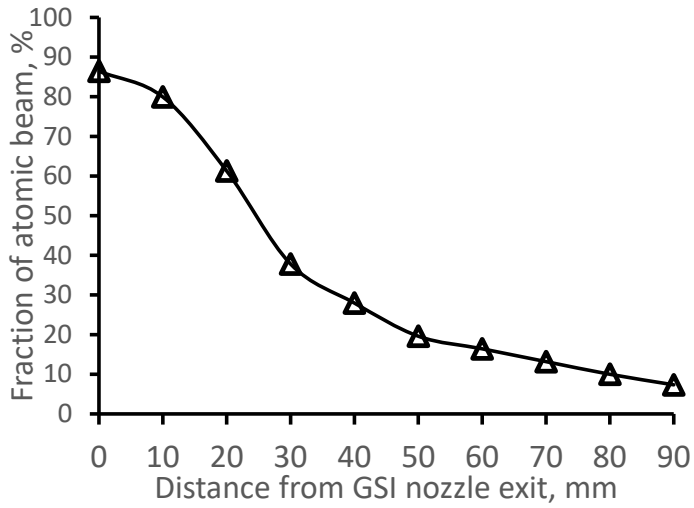

Figure 5. Results of the Monte-Carlo trajectory simulations of the fraction extracted from the gas cell ^{164}Dy atomic beam inside the region of 10 mm (the Laser-1 beam diameter) as a function of distance from GSI nozzle exit. The number of calculated atoms is 10,000.

Figure 6 demonstrates how the calculated longitudinal velocity spread of the dysprosium atomic beam depends on the distance from the GSI nozzle. The data averaged in the radial plane over the Laser-1 beam diameter makes it possible to compare our calculations directly and simply with future experiments at the JetRIS setup. Moreover, such calculations allow for getting crucial quantitative information on the quality of the cooled in the supersonic gas jet atomic beams.

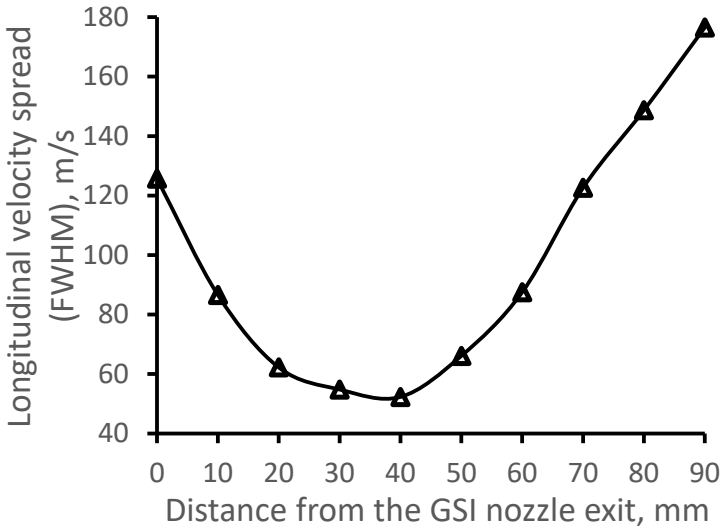

Figure 6. Results of the Monte-Carlo trajectory simulations for ^{164}Dy atomic beam longitudinal velocity spread (FWHM) as a function of the distance from GSI nozzle exit. The data averaged in the radial plane for the Laser-1 beam diameter of 10 mm. Number of calculated atoms is 10,000.

Figures 7 and 8 illustrate the distributions of longitudinal and radial ^{164}Dy atomic beam velocity components (averaged in the radial plane for the Laser-1 beam diameter of 10 mm) for different distances from the GSI nozzle.

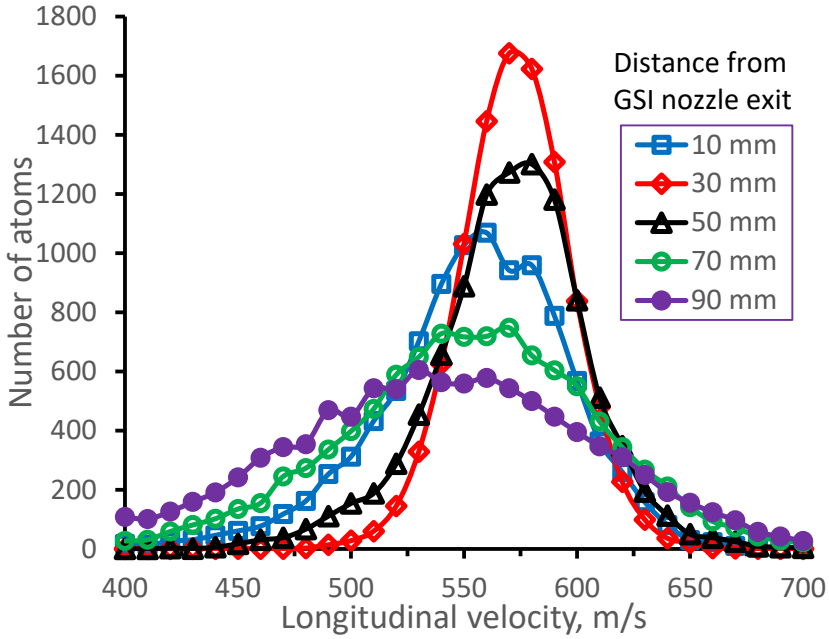

Figure 7. Results of the Monte-Carlo trajectory simulations for ^{164}Dy atomic beam longitudinal velocity distributions (averaged in the radial plane for the Laser-1 beam diameter of 10 mm) for different distances from GSI nozzle exit. The number of calculated atoms for each velocity distribution is 10,000.

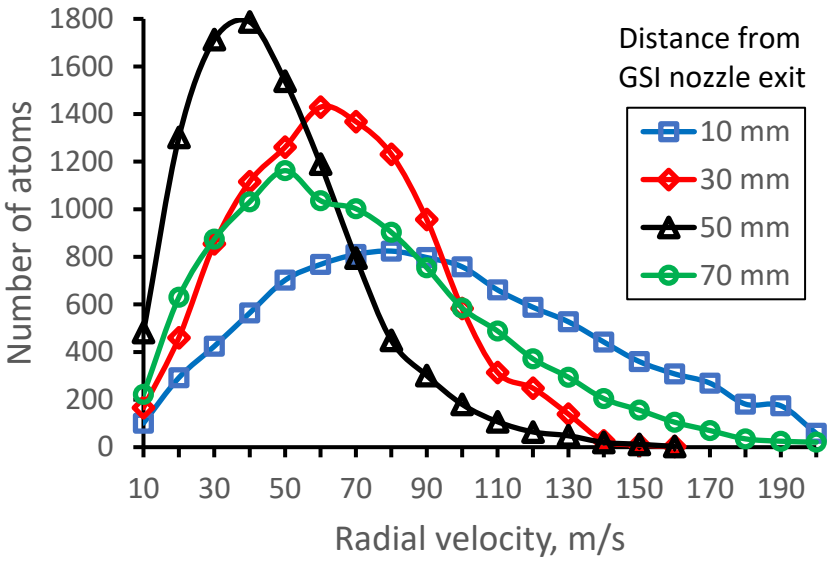

Figure 8. Results of the Monte-Carlo trajectory simulations for ^{164}Dy atomic beam radial velocity distributions (averaged in the radial plane for the Laser-1 beam diameter of 10 mm) for different distances from GSI nozzle exit. The number of calculated atoms for each velocity distribution is 10,000.

2.3. GSI Nozzle at Gas Cell Pressure P_{cell} = 50 mbar and P_{bg} = 3.23 × 10^{-2} mbar

To check how the supersonic gas jet structure and parameters extracted into the jet ^{164}Dy atomic beam will look at lower stagnation gas cell pressure, we performed calculations, which are similar to the calculations described above in Section 2.2 for the same pumping capacity, but for the gas cell pressure of P_{cell} = 50 mbar. The results of the gas dynamic simulation for argon gas density, temperature, velocity, and Mach number flow fields for the GSI nozzle at P_{cell} = 50 mbar are shown in Figure 9.

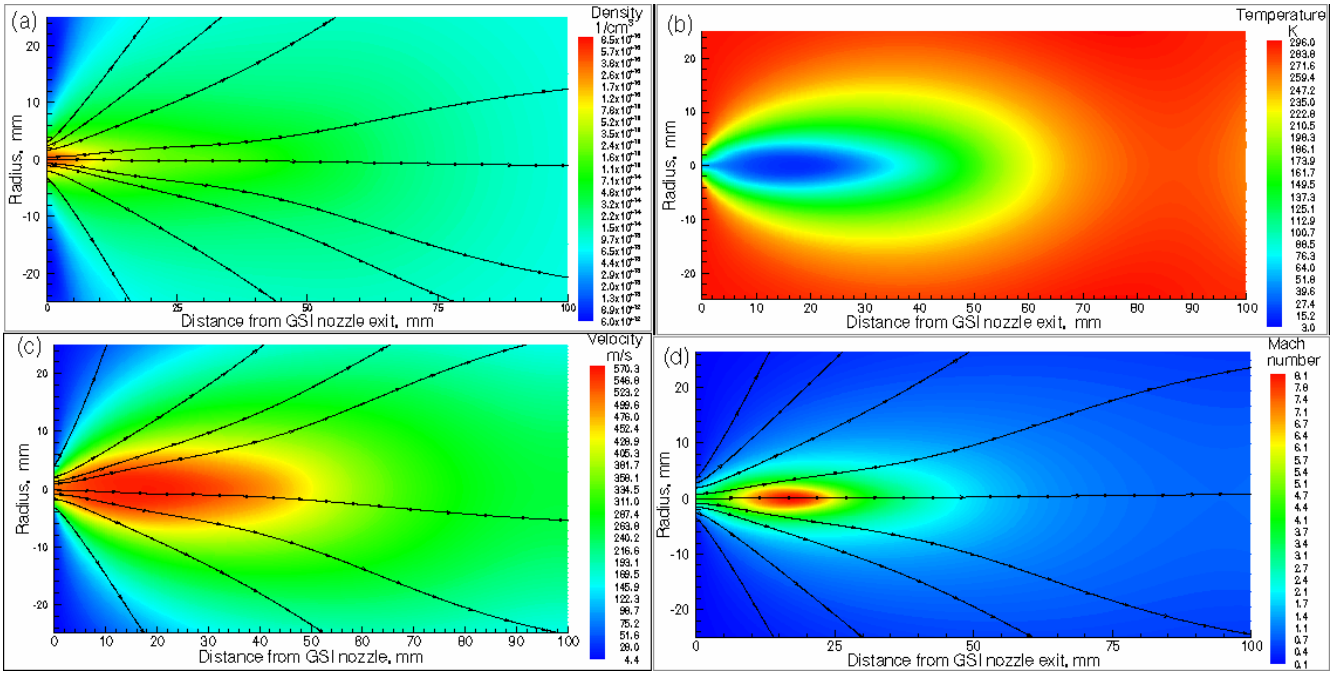

Figure 9. Results of the gas dynamic simulation: (**a**) density, (**b**) temperature, (**c**) velocity and (**d**) Mach number flow fields for GSI nozzle. The stagnation pressure and temperature in the gas cell are P_{cell} = 50 mbar and T_{cell} = 296 K, correspondingly. Background pressure in the gas-jet chamber is P_{bg} = 3.23 × 10^{-3} mbar. Black arrowed lines show the gas flow directions.

Results of the Monte Carlo simulations for the case of 50 mbar gas cell pressure are shown in Figures 10 and 11. In addition, we have included the results of calculations presented above in Figures 5 and 6 for the case of P_{cell} = 100 mbar for comparison. Notice that the atomic beam diffusion losses inside the GSI nozzle at P_{cell} = 50 mbar are equal to 27.7 ± 0.8%, about factor 2 higher than that at P_{cell} = 100 mbar.

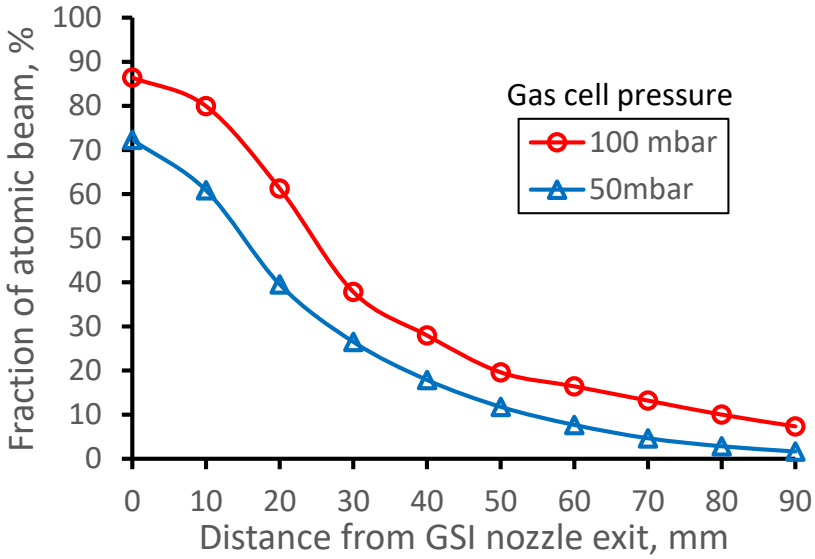

Figure 10. Results of the Monte-Carlo trajectory simulations of the fraction extracted from the gas cell ^{164}Dy atomic beam inside the region of 10 mm in diameter (it is the Laser-1 diameter) as a function of distance from GSI nozzle exit. Number of calculated atoms is 10,000.

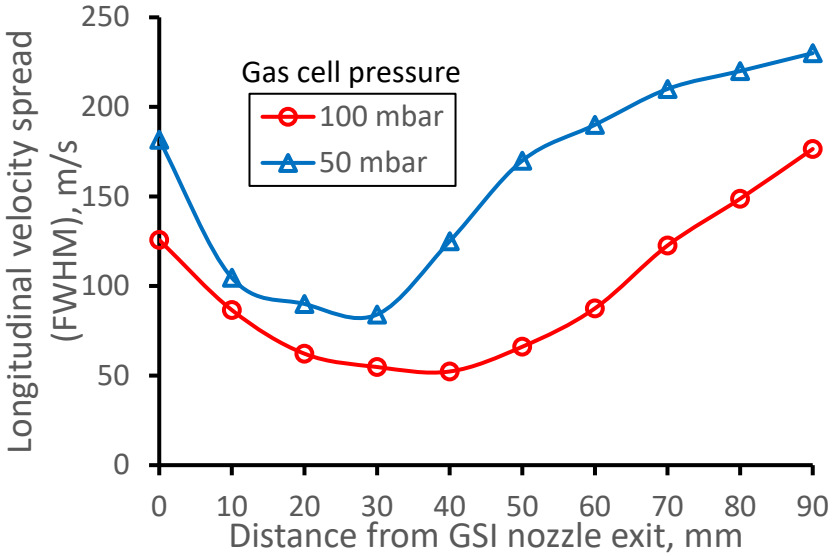

Figure 11. Results of the Monte-Carlo trajectory simulations for ^{164}Dy atomic beam longitudinal velocity spread (FWHM) as a function of distance from GSI nozzle exit. The data averaged in the radial plane for the Laser-1 beam diameter of 10 mm. Number of calculated atoms is 10,000.

3. Results for Double-Nozzle Technique

3.1. Historical Notes

The new double-nozzle technique for in-gas-jet resonance ionization laser spectroscopy we propose here is based on gas dynamic cooling of low-energy molecular and ion beams. This idea was proposed for the first time in 1979 [52,53] and described also, e.g., in [5,39,54–61]. It consists of direct injection of primary beams into supersonic carrier gas jet using a specially designed supersonic nozzle. The converging–diverging supersonic nozzle has a narrow

inner tube on its axis which passes through a gas stagnation chamber into a region of supersonic carrier gas expansion (see Figure 12). Then, this inner tube particle of interest is injected into the expanded supersonic gas jet. A low-pressure zone forms immediately after the tube, so this supersonic carrier gas jet acts as a vapor-jet pump. It provides for the possibility of effective differential pumping in the case of ion beam injection [60].

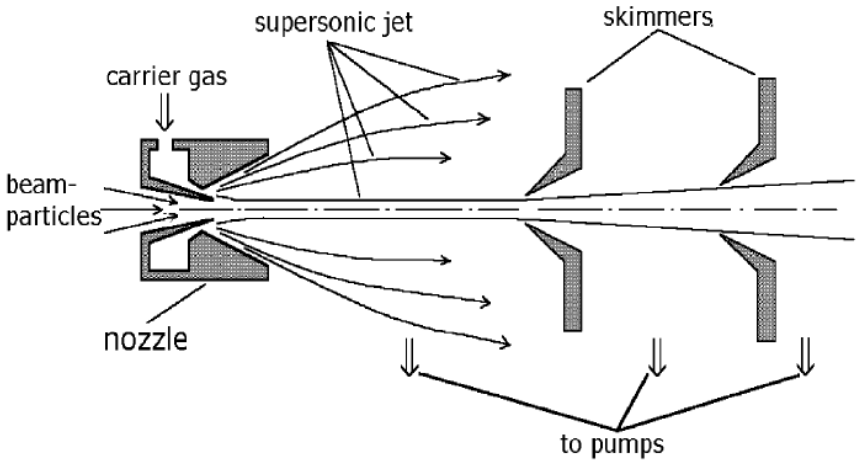

Figure 12. Schematic of the method of gas dynamic cooling of low-energy molecular and ion beams. Picture from Refs. [39,61]. See the text for details.

To show the feasibility and effectivity of the described gas dynamic method experimentally. A gas dynamic molecular beam source setup was constructed in the middle of the 1980s at the Leningrad Nuclear Physics Institute (LNPI) in Gatchina [56,57]. As a result of experimental investigations, it has been obtained the effective cooling of hot lead iodine (PbI) molecular beam in the supersonic nitrogen jet from 900 K down to 20 K was an essential part of our PhD work [54]. Notice that the two-atomic molecules PbI are free radicals produced via the thermal decomposition of three-atomic molecules PbI_2 inside the separately heated thin quartz capillary installed into the inner tube of the supersonic nozzle shown in Figure 12.

The description and schematic layout with photos of some parts of this gas dynamic molecular beam source setup in LNPI one can find in our presentation at Institute for Medium Energy Physics (IMEP) (renamed after 2004 to "Stefan Meyer Institute" (SMI)), Vienna [61].

3.2. Double-Nozzle Design

To implement the proposed here double-nozzle technique for in-gas-jet laser resonance ionization spectroscopy, it is sufficient to connect the short conical convergent-divergent nozzle of the gas cell, which we will call the 1st nozzle, with the 2nd nozzle, which designs schematically shown in Figure 12.

Schematic views of the double-nozzle design combined with results of the gas dynamic simulation for argon temperature and velocity flow fields are shown in Figures 13 and 14, correspondingly.

A gas vortex that one can see in Figures 13 and 14 appears in the region between the 1st nozzle throat and the exit of the inner tube in the 2nd nozzle due to the viscous gas jet interaction with the walls. This vortex around the supersonic jet flowing out of the gas cell protects the dysprosium atoms from hitting the walls, thus reducing the diffusion losses of the neutral atomic beam extracted from the gas cell. The result of the Monte Carlo calculation shows that only $9.5 \pm 0.4\%$ of the removed from the gas cell atomic beam is lost inside this double-nozzle device.

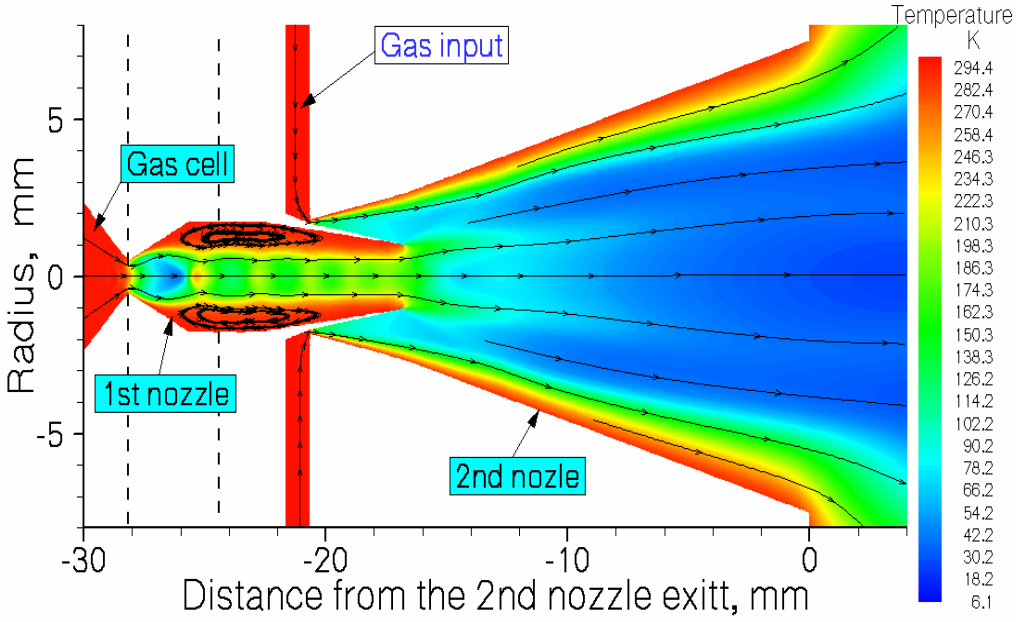

Figure 13. Schematic view of the double-nozzle design combined with the gas dynamic simulation results for argon temperature flow field. The stagnation gas cell pressure P_{cell} = 100 mbar, gas input (stagnation) pressure P_{noz} = 81 mbar, background presses in the vacuum gas-jet chamber $P_{bg} = 2.0 \times 10^{-2}$ mbar for the pumping capacity of 1300 l/s. The temperature of the gas cell and nozzles is 296 K. Black arrowed lines show the gas flow directions. Two black dashed vertical lines designate a possible connection of flanges for assembling this double-nozzle device.

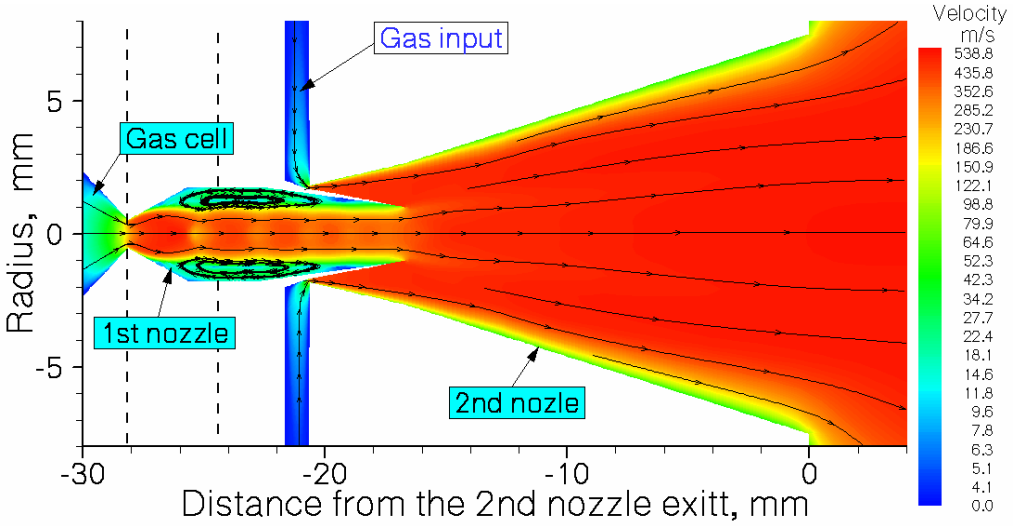

Figure 14. A schematic view of the double-nozzle design is shown in Figure 13 but combined with the results of the gas dynamic simulation for the argon velocity flow field.

The main design parameters of the double-nozzle device used in simulations are listed in Table 1.

3.3. Double-Nozzle at P_{cell} = 100 mbar, P_{noz} = 81 mbar and $P_{bg} = 2 \times 10^{-2}$ mbar

Results of the gas dynamic simulation for argon gas density, temperature, velocity, and Mach number flow fields for the double-nozzle are shown in Figure 15.

Table 1. Main design parameters of the double-nozzle device.

1st Nozzle	
Exit diameter	3.5 mm
Throat diameter	1.0 mm
Length of diverging cone	2.5 mm
Connection tube between the 1st and 2nd nozzle	
Tube diameter	3.5mm
Tube length	3.0 mm
Inner tube in the 2nd nozzle	
Exit diameter	2.0 mm
Inner entrance diameter	3.5 mm
Inner total length	6.0 mm
Supersonic part length	4.0 mm
Out entrance diameter	4.0 mm
Outer total length	5.0 mm
Diverging 2nd nozzle	
Throat diameter	3.6 mm
Diverging cone length	20. mm
Exit diameter	15.0 mm
Annual gap between nozzle throat and inner tube	0.1 mm

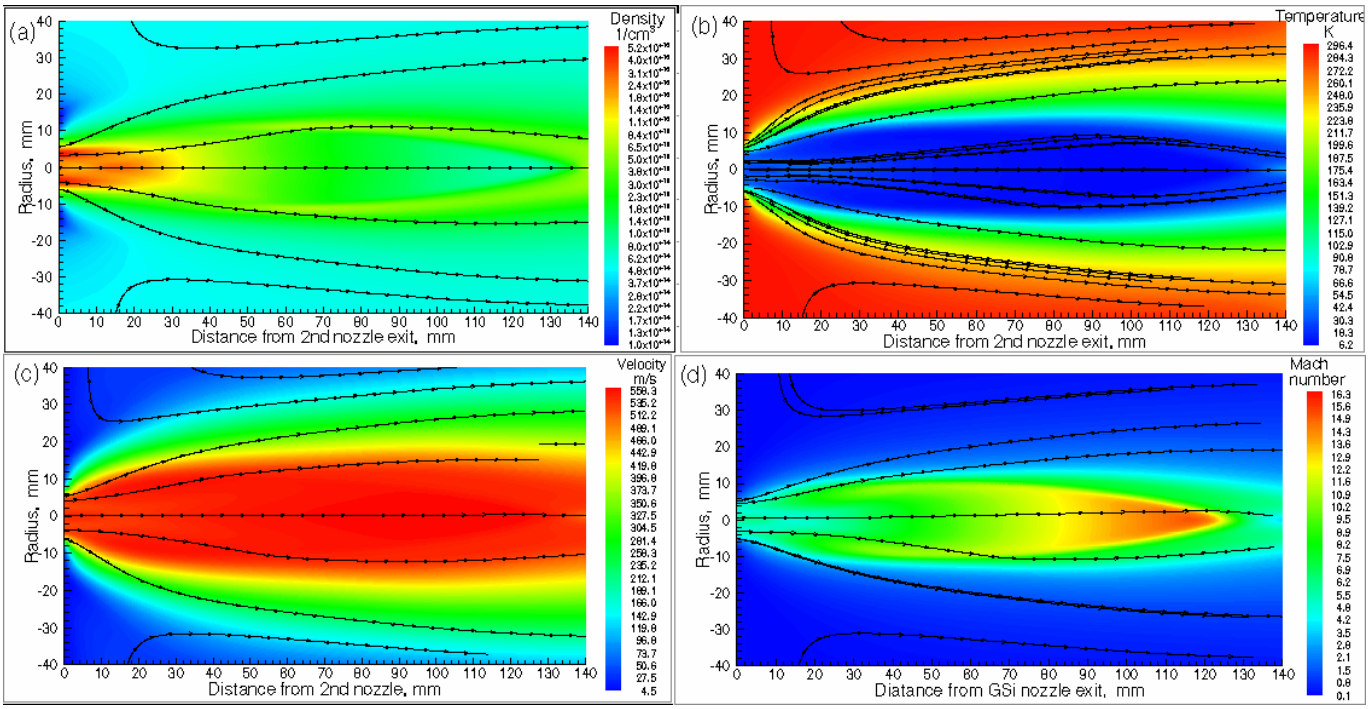

Figure 15. Results of the gas dynamic simulation: (**a**) density, (**b**) temperature (**c**) velocity and (**d**) Mach number flow fields for the double-nozzle. The stagnation gas cell pressure P_{cell} = 100 mbar, gas input (stagnation) pressure P_{noz} = 81 mbar, background pressure in the vacuum gas-jet chamber $P_{bg} = 2.0 \times 10^{-2}$ mbar for the pumping capacity of 1300 l/s. The temperature of the gas cell and both nozzles is 296 K. Black arrowed lines show the gas flow direction.

Results of the Monte-Carlo simulations for the ^{164}Dy atomic beam extracted from the gas cell using the double-nozzle technique are shown in Figures 16–19.

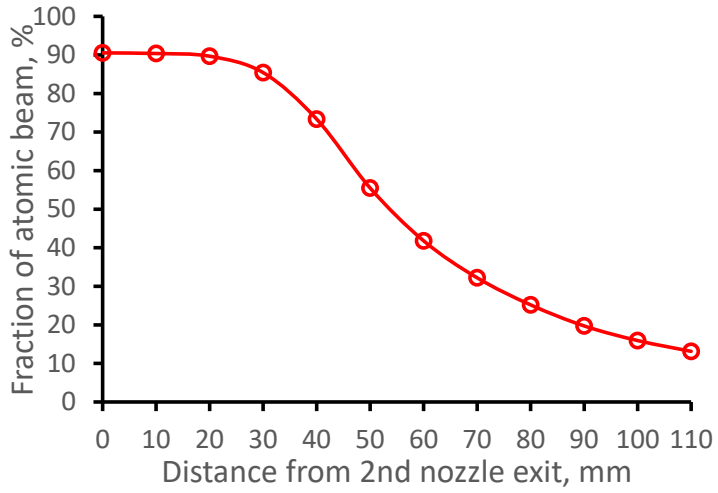

Figure 16. Results of the Monte-Carlo trajectory simulations of the fraction extracted from the gas cell ^{164}Dy atomic beam inside the gas jet of 10 mm diameter (Laser-1 diameter) as a function of distance from the 2nd nozzle exit. Number of calculated atoms is 10,000.

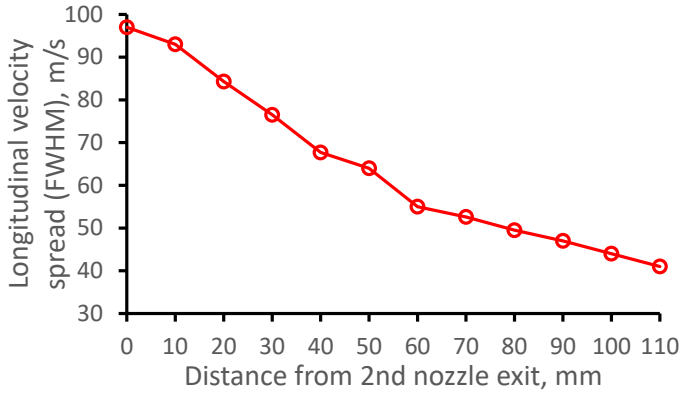

Figure 17. Results of the Monte-Carlo trajectory simulations for ^{164}Dy atomic beam longitudinal velocity spread (FWHM) as a function of the distance from the 2nd nozzle exit. The data averaged in the radial plane for the Laser-1 beam diameter of 10 mm. Number of calculated atoms is 10,000.

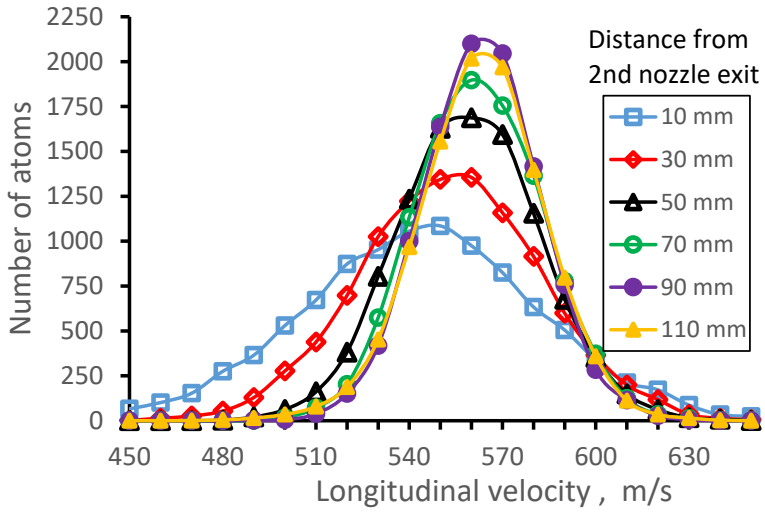

Figure 18. Results of the Monte-Carlo trajectory simulations for ^{164}Dy atomic beam longitudinal velocity distributions (averaged in the radial plane for the Laser-1 beam diameter of 10 mm) for different distances from the 2nd nozzle exit. The number of calculated atoms for each velocity distribution is 10,000.

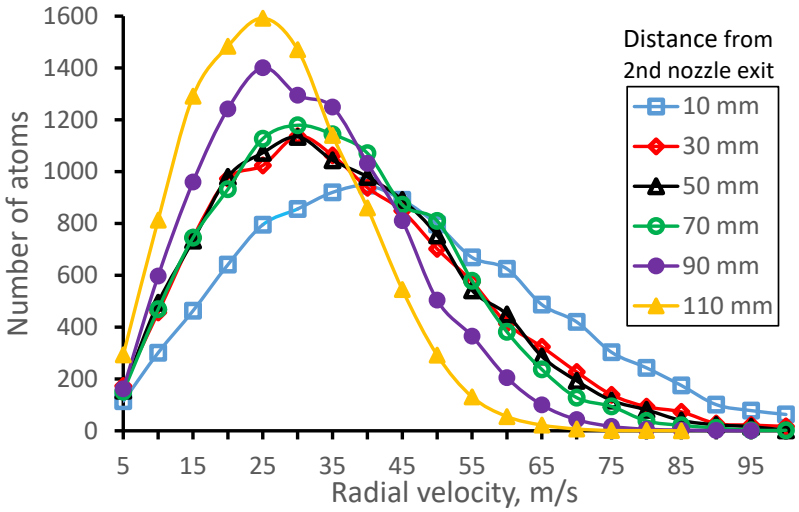

Figure 19. Results of the Monte-Carlo trajectory simulations for ^{164}Dy atomic beam radial velocity distributions (averaged in the radial plane for the Laser-1 beam diameter of 10 mm) for different distances from the 2nd nozzle exit. The number of calculated atoms for each velocity distribution is 10,000.

3.4. Effect of the Pumping Speed

To investigate the effect of the pumping speed on the ^{164}Dy atomic beam parameters in the supersonic gas jet at fixed stagnation pressures P_{cell} = 100 mbar, P_{noz} = 81 mbar, we have made corresponding gas dynamic and Monte Carlo simulations.

In addition to the previously considered variant of 1300 l/s pumping speed (it corresponds to $P_{bg} = 2 \times 10^{-2}$ mbar), we have performed calculations for the pumping speed of 2600 l/s ($P_{bg} = 1 \times 10^{-2}$ mbar) and 650 l/s ($P_{bg} = 4 \times 10^{-2}$ mbar). The results of these calculations are presented in following Figures 20–22. To provide a simple and direct comparison of the double-nozzle technique with the case of the GSI nozzle, we have included the results of calculations for the GSI setup [32,33] presented above in Section 2.

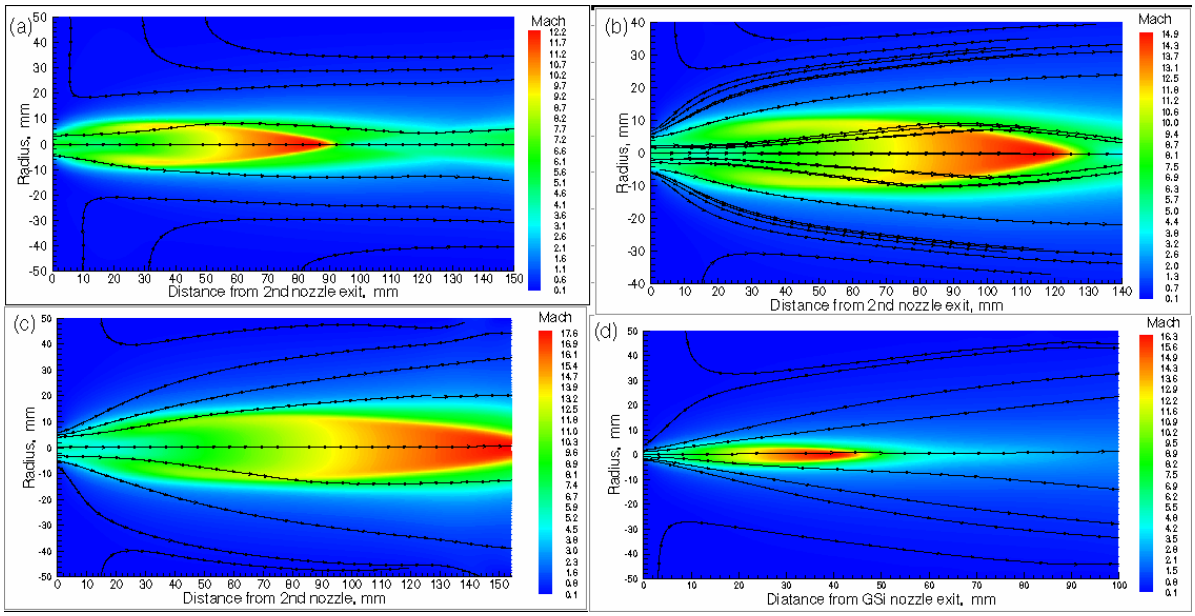

Figure 20. Results of the gas dynamic simulation for Mach number flow fields for double nozzle at different pumping speeds: (**a**) 650 l/s, (**b**) 1300 l/s, (**c**) 2600 l/s, (**d**) GSI nozzle. The stagnation gas cell pressure P_{cell} = 100 mbar, gas input (stagnation) pressure P_{noz} = 81 mbar. The temperature of the gas cell and both nozzles is 296 K. Black arrowed lines show the gas flow direction.

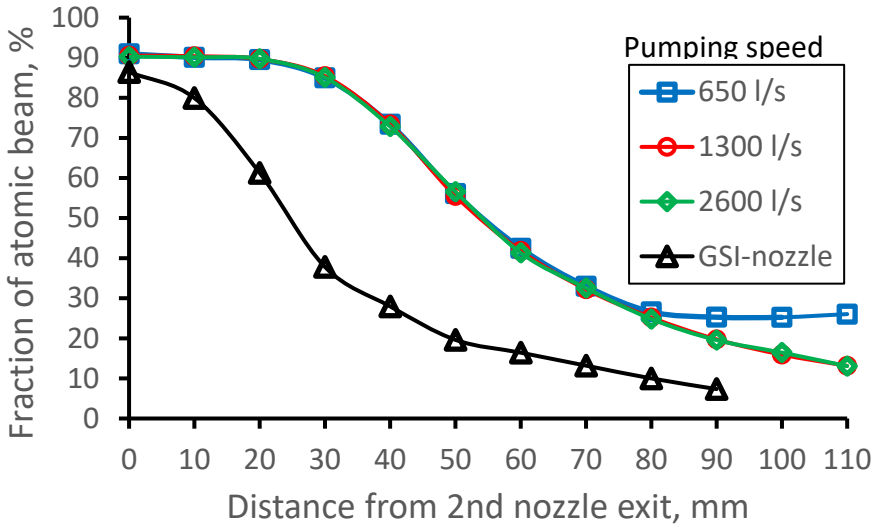

Figure 21. Results of the Monte-Carlo trajectory simulations of the fraction of the extracted from the gas cell ^{164}Dy atomic beam inside the gas jet of 10 mm in diameter (it is the Laser-1 diameter) for different pumping speeds as a function of distance from the 2nd nozzle exit. Number of calculated atoms is 10,000 for each variant.

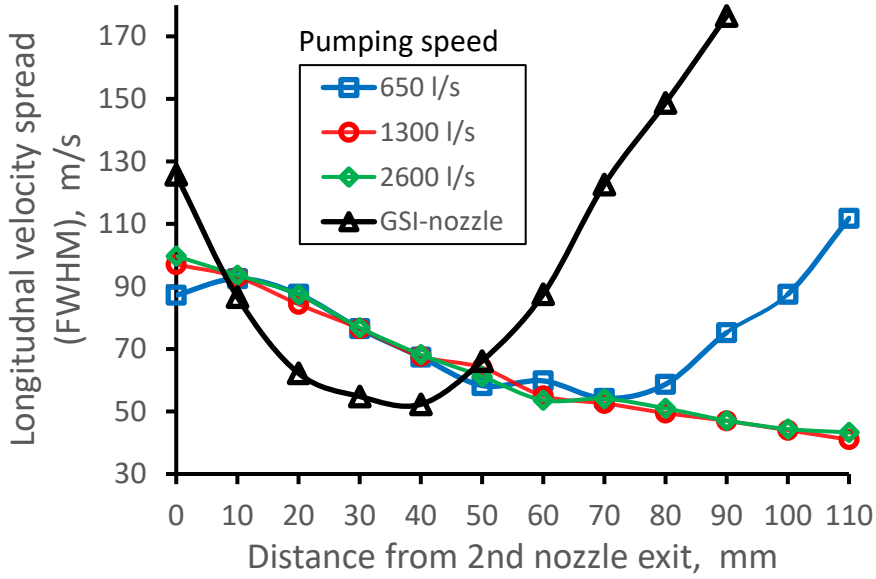

Figure 22. Results of the Monte-Carlo trajectory simulations for ^{164}Dy atomic beam longitudinal velocity spread (FWHM) for different pumping speeds as a function of the distance from the 2nd nozzle exit. The data averaged in the radial plane for the Laser-1 beam diameter of 10 mm. Number of calculated atoms is 10,000 for each variant.

3.5. Effect of the Input (Stagnation) Pressure in the 2nd Nozzle

To make sure that the proposed here double-nozzle technique works effectively in a wide range of input pressures in the 2nd nozzle, we performed, in addition, gas dynamic and Monte Carlo simulations for two other pressures P_{noz} and at fixed gas cell pressure P_{cell} = 100 mbar and pumping capacity of 1300 l/s. These variants are P_{noz} = 162 mbar (the corresponding $P_{bg} = 3 \times 10^{-2}$ mbar) and P_{noz} = 263 mbar (the corresponding $P_{bg} = 4 \times 10^{-2}$ mbar).

The results of these Monte Carlo calculations are presented in Figures 23 and 24. The corresponding results for the case of the GSI nozzle we added for illustration and comparison.

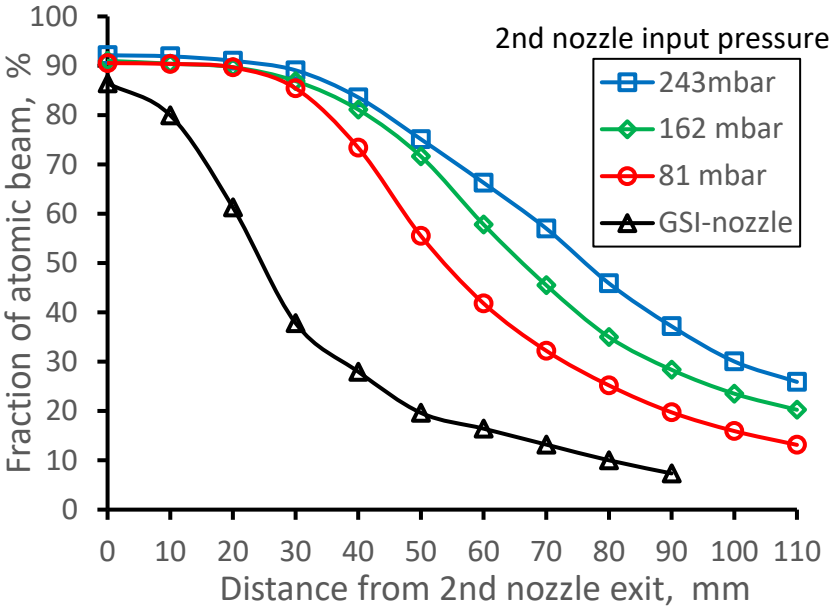

Figure 23. Results of the Monte-Carlo trajectory simulations of the fraction of the extracted from the gas cell ^{164}Dy atomic beam inside the region of 10 mm in diameter (it is the Laser-1 diameter) for different input pressures P_{noz} as a function of distance from the 2nd nozzle exit. Number of calculated atoms is 10,000 for each variant.

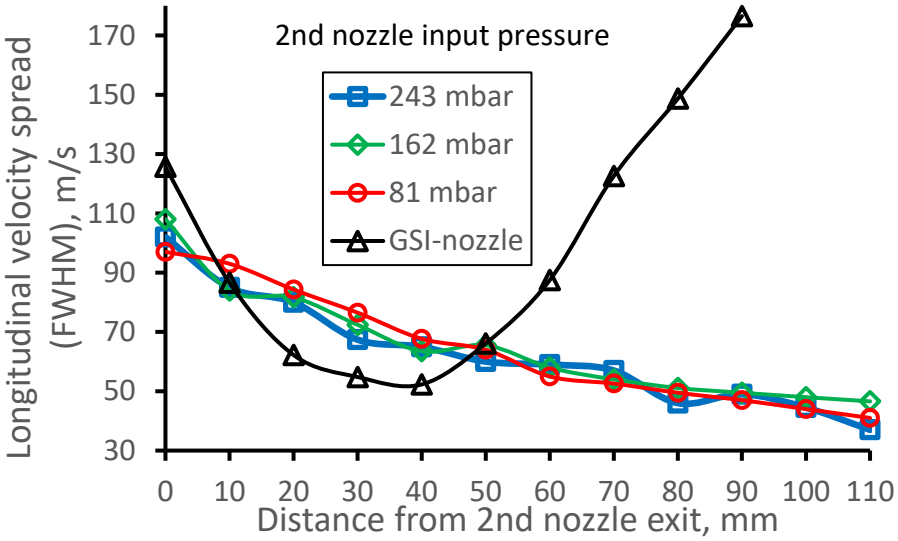

Figure 24. Results of the Monte-Carlo trajectory simulations for ^{164}Dy atomic beam longitudinal velocity spread (FWHM) for different input pressures P_{noz} as a function of the distance from the 2nd nozzle exit. The data averaged in the radial plane for the Laser-1 beam diameter of 10 mm. Number of calculated atoms is 10,000 for each variant.

3.6. Effect of the Stagnation Pressure in the Gas Cell

To see how the double-nozzle technique will work at twice less stagnation pressure in the gas cell, we performed gas dynamic and Monte Carlo simulation for the case of P_{cell} = 50 mbar and input gas pressure P_{noz} = 81 mbar. The pumping capacity of 1300 l/s corresponds to $P_{bg} = 1.5 \times 10^{-2}$ mbar.

The Monte Carlo calculation results are presented in Figures 25 and 26. The corresponding results for the previously considered case of stagnation P_{cell} = 100 mbar and $P_{bg} = 2 \times 10^{-2}$ mbar we added for illustration and comparison.

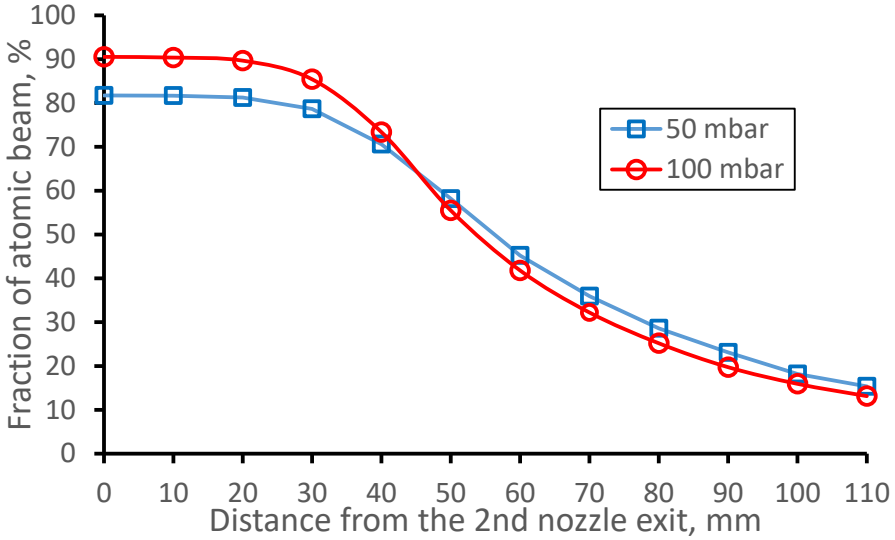

Figure 25. Results of the Monte-Carlo trajectory simulations of the fraction of the extracted from the gas cell ^{164}Dy atomic beam inside the region of 10 mm in diameter (it is the Laser-1 diameter) for two different gas cell pressures P_{cell} as a function of distance from the 2nd nozzle exit. Number of calculated atoms is 10,000 for each variant.

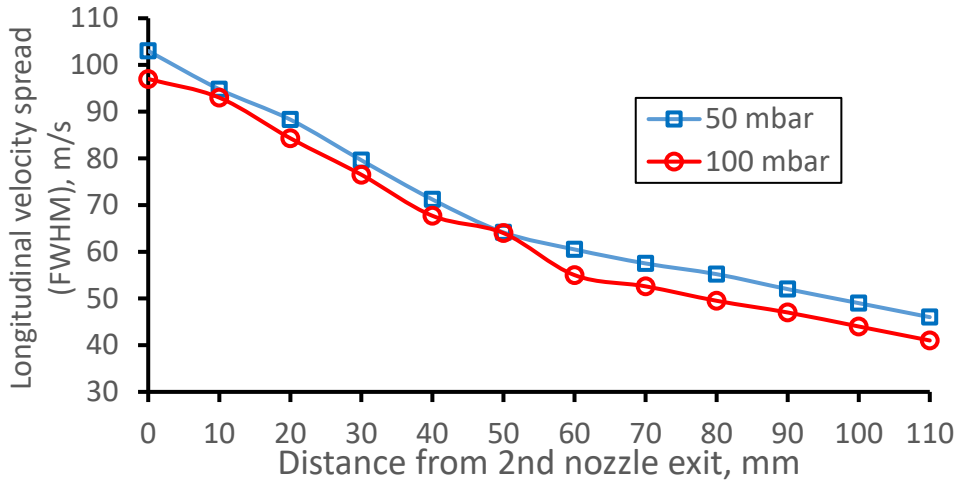

Figure 26. Results of the Monte-Carlo trajectory simulations for ^{164}Dy atomic beam longitudinal velocity spread (FWHM) for different input pressures P_{noz} as a function of the distance from the 2nd nozzle exit. The data averaged in the radial plane for the Laser-1 beam diameter of 10 mm. Number of calculated atoms is 10,000 for each variant.

Notice that the calculated diffusion losses of the atomic beam inside the double-nozzle device at P_{cell} = 50 mbar is 18.3 $\pm$ 0.6%, a factor of 2 higher than that for P_{cell} = 100 mbar, and it looks reasonable. Nevertheless, the data for two different P_{cell} values look very similar in Figures 25 and 26. For comparison, it is not so for the GSI nozzle (see Figures 10 and 11).

3.7. Effect of the Laser-1 Beam Diameter

When the distance between adjacent rods of the curved RFQ (the curved RFQ allows for the axial Laser-1 beam injection into the gas jet) is less than considered above the laser beam diameter of 10 mm, one should use the Laser-1 beam of a smaller diameter.

It is essential to know how the JetRIS (or any other similar project) overall efficiency and quality of the extracted into gas jet atomic beam depend on the Laser-1 beam diameter. Some information about one can get from the results of our Monte Carlo simulations shown in Figures 27 and 28.

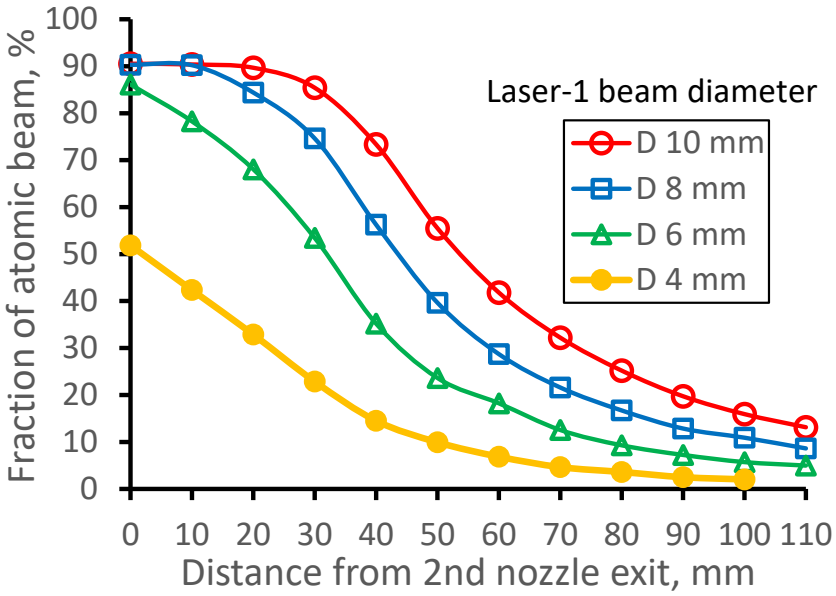

Figure 27. Results of the Monte-Carlo trajectory simulations of the fraction extracted from the gas cell ^{164}Dy atomic beam for different Laser-1 beam diameters as a function of distance from the 2nd nozzle exit. Number of calculated atoms is 10,000 for each variant.

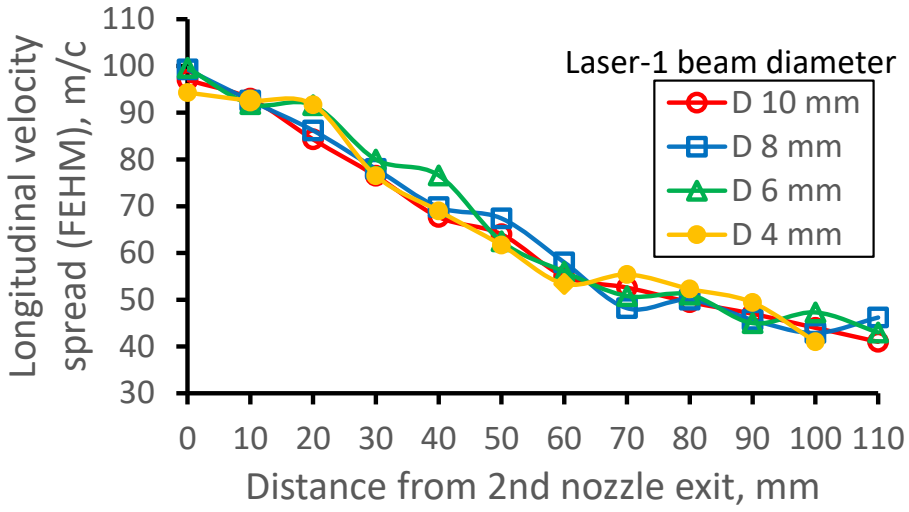

Figure 28. Results of the Monte-Carlo trajectory simulations for ^{164}Dy atomic beam longitudinal velocity spread (FWHM) for different Laser-1 beam diameters as a function of the distance from the 2nd nozzle exit. The data averaged in the radial plane for each Laser-1 beam diameter. Number of calculated atoms is 10,000 for each variant.

3.8. Monte Carlo Simulations for Nobelium Atoms in the Gas Jet

The goal of the JetRIS project [32,33] under development at GSI is the study of the nuclear properties of nobelium isotopes with high precision by laser spectroscopy in an argon supersonic gas jet. That is why we performed, in addition, a Monte Carlo simulation for ^{253}No isotope, as well. For the Monte Carlo simulation of the nobelium atomic beam in a supersonic gas jet, we used the same results of gas dynamic simulation (see Figure 15) for the ^{164}Dy atomic beam. These results are shown in Figures 29–31. Results for the ^{164}Dy we added for comparison.

As shown in Figure 29, the decrease of the beam fractions with the distance from the 2nd nozzle exit is near the same for both dysprosium and nobelium atomic beams. It reflects that thermalized argon dysprosium and nobelium atoms equally follow the supersonic jet expansion. At the same time, the longitudinal velocity spreads shown in Figure 30 are

different. It explains by the mass difference of ^{164}Dy and ^{253}No atoms because the velocity spread of the atomic beam thermalized in the gas should be inversely proportional to the square root of the atom mass.

Figure 31 shows the ^{253}No atomic beam longitudinal velocity distributions for different distances from the 2nd nozzle exit for illustration.

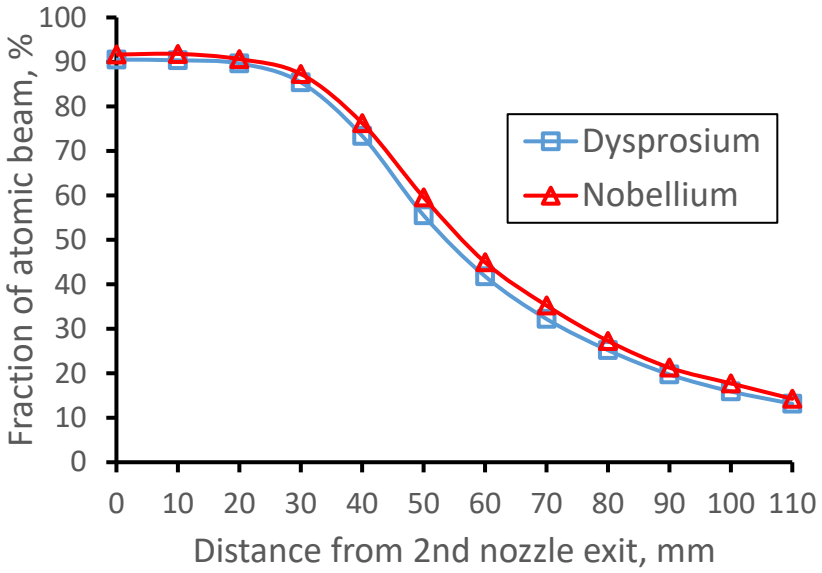

Figure 29. Results of the Monte-Carlo trajectory simulations of the fraction of the extracted from the gas cell ^{253}No atomic beam inside the gas jet of 10 mm in diameter (it is the Laser-1 diameter) for the gas cell pressure P_{cell} = 100 mbar, P_{noz} = 81 mbar and $P_{bg} = 2 \times 10^{-2}$ mbar as a function of distance from the 2nd nozzle exit. Number of calculated atoms is 10,000 for each case.

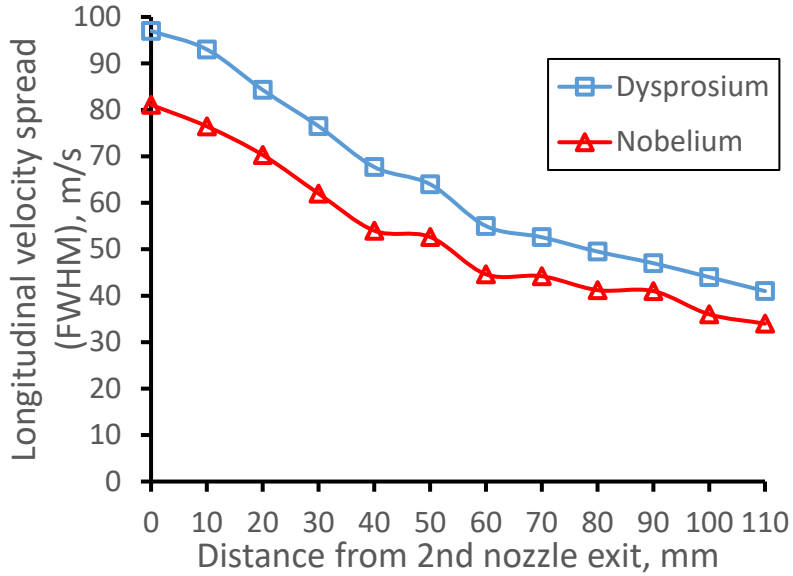

Figure 30. Results of the Monte-Carlo trajectory simulations for ^{253}No atomic beam longitudinal velocity spread (FWHM) for the gas cell pressure P_{cell} = 100 mbar, P_{noz} = 81 mbar and $P_{bg} = 2 \times 10^{-2}$ mbar as a function of the distance from the 2nd nozzle exit. The data averaged in the radial plane for the Laser-1 beam diameter of 10 mm. Number of calculated atoms is 10,000 for each case.

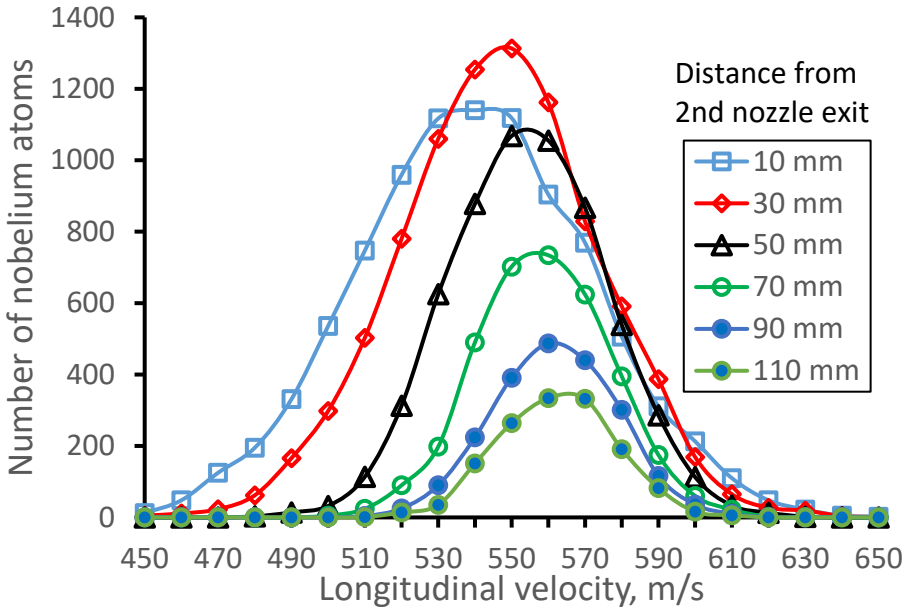

Figure 31. Results of the Monte-Carlo trajectory simulations for ^{253}No atomic beam longitudinal velocity distributions (averaged in the radial plane for the Laser-1 beam diameter of 10 mm) for different distances from the 2nd nozzle exit. The number of calculated atoms for each velocity distribution is 10,000.

4. Discussion and Outlook

In Section 2 of the article, we have investigated by means of detailed computer experiments the conventional nowadays technique of the so-called in-gas-jet laser resonance ionization spectroscopy. As a typical representative of this technique, we have chosen for the numerical computer analysis the setup of the JetRIS project [32,33]. The JetRIS project is under development now at GSI, Darmstadt.

Results of the gas dynamic simulation for the exit flow channel of 12 mm in diameter are presented in Figures 1 and 2. It is a laminar gas flow with a Reynolds number of 123. The calculated Monte Carlo simulation time-of-flight of evaporated 164Dy neutral atoms from the hot filament tip to the nozzle throat is 7.0 ± 1.4 ms (see Figure 3), the extraction efficiency is 94.5 ± 2.7%, or in other words, the atomic beam diffusion losses are equal to 5.5 ± 0.3%. The gas dynamic + Monte Carlo simulations show that the additional diffusion losses of the 164Dy atomic beam inside the GSI nozzle at P_{cell} = 100 mbar are equal to 15.6 ± 0.6%. The graphic description of the calculated argon supersonic jet (flow fields of gas density, velocity, temperature, and Mach number) flowing out of the GSI nozzle into the gas-jet chamber is shown in Figures 4 and 9 for the gas cell pressure of 100 mbar and 50 mbar, correspondingly. Here the strong effect of the gas viscosity of the supersonic jet structure and parameters is visible.

Notice that the 164Dy atomic beam diffusion losses inside the GSI nozzle for P_{cell} = 50 mbar 27.7 ± 0.8% are considerably higher than that at P_{cell} = 100 mbar, which looks reasonable. Moreover, the production efficiency of excited by the Laser-1 dysprosium atoms in the gas jet is also less in the case of P_{cell} = 50 mbar (see Figure 10). As a result, the atomic beam quality, shown in Figure 11 as a longitudinal velocity spread, is also worse.

Section 3 of the article describes and explores our proposal for a new double-nozzle technique. By means of gas dynamics and Monte Carlo simulations, we have shown that this new technique has many advantages over the conventional technique described in Section 2 of the article. E.g., the atomic beam diffusion losses inside the double-nozzle system are equal only to 9.5 ± 0.4%, which is in factor 1.6 less than in the case of the use of GSI nozzle at the same gas cell pressure (P_{cell} = 100 mbar) and having the same nozzle throat diameter of 1.0 mm. The double nozzle method is much more efficient (see the direct comparison in Figures 16, 21 and 23), and it also allows obtaining better atomic beam

quality (expressed in longitudinal velocity spread) for a longer downstream distance from the 2nd nozzle exit (see the direct comparison in Figures 17, 22 and 24).

The proposed double-nozzle technique can effectively work in various P_{cell} and Pnoz pressures. Therefore, there is no need here for the use of any butterfly valve placed in front of the vacuum pump, as it is in [32] to adjust the background pressure in the gas-jet chamber under changing the P_{cell} or using the nozzles having different throat diameters and profiles of its diverging supersonic part. The butterfly valve allows for decreasing the nominal capacity of the used vacuum pump, but it cannot increase it when required.

Moreover, the double-nozzle design we suggest in the JetRIS setup at GSI, whose main parameters are listed in Table 1, can be effectively used at different vacuum pump capacities (see Section 3.4 above).

To help the authors of works [32,33] prepare for the future online measurement of nobelium isotopes, we also performed the Monte Carlo simulations for the 253No atomic beam in the argon supersonic jet. The results of these calculations, which are presented in Section 3.7, allow us to quantitatively estimate the efficiency of the JetRIS setup operation using the proposed double-nozzle technique.

Implementing the proposed double-nozzle technique to the JetRIS setup will be enough to replace the present GSI nozzle with the double-nozzle system presented in the article.

In conclusion, we can say that the double-nozzle design, which main parameters are listed in Table 1, can also be used for other similar setups or/and projects. If, e.g., operation conditions or specific requirements to these setups/projects are very different from that in the JetRIS setup, then we can make similar computer experiments to find an optimal solution for these cases upon the corresponding request.

Funding: This research received no external funding.

Data Availability Statement: The data presented in this study are available upon request from the corresponding author.

Conflicts of Interest: The author declares no conflict of interest.

References

1. Dendooven, P. The development and status of the IGISOL technique. *Nucl. Instrum. Methods Phys. Res. B* **1997**, *126*, 182–189. [CrossRef]
2. Äystö, J. Development and applications of the IGISOL technique. *Nucl. Instrum. Methods Phys. Res. A* **2001**, *693*, 477–494. [CrossRef]
3. Moore, I.D.; Dendooven, P.; Ärje, J. The IGISOL technique—Three decades of development. *Hyperfine Interact* **2014**, *223*, 17–62. [CrossRef]
4. Schwarz, S.; Bollen, G.; Lawton, D.; Lofy, P.; Morrissey, D.J.; Ottarson, J.; Ringle, R.; Schury, P.; Sun, T.; Varentsov, V.; et al. The low-energy-beam and ion-trap facility at NSCL/MSU. *Nucl. Instrum. Methods Phys. Res. B* **2003**, *204*, 507–511. [CrossRef]
5. Varentsov, V.L.; Habs, D. A cooler for intense low-energy ion beams. *Nucl. Instrum. Methods Phys. Res. A* **2003**, *496*, 286–292. [CrossRef]
6. Varentsov, V.L.; Habs, D. Fair-wind gas cell—A new concept of a buffer gas cell design. *Nucl. Instrum. Methods Phys. Res. A* **2002**, *490*, 16–29. [CrossRef]
7. Sonoda, T.; Fujita, M.; Yamazaki, A.; Endo, T.; Shinozuka, T.; Miyashita, Y.; Sato, N.; Goto, A.; Tanaka, E.; Suzuki; et al. Development of the RF-IGISOL at CYRIC. *Nucl. Instrum. Methods Phys. Res. B* **2007**, *254*, 295–299. [CrossRef]
8. Moore, I.D. New concepts for the ion guide technique. *Nucl. Instrum. Methods Phys. Res. B* **2008**, *266*, 4434–4441. [CrossRef]
9. Sonoda, T.; Wada, M.; Tomita, H.; Sakamoto, C.; Takatsuka, T.; Furukawa, T.; Iimura, H.; Ito, Y.; Kubo, T.; Matsuo, Y.; et al. Development of a resonant laser ionization gas cell for high-energy, short-lived nuclei. *Nucl. Instrum. Methods Phys. Res. B* **2013**, *295*, 1–10. [CrossRef]
10. Schury, P.; Wada, M.; Ito, Y.; Arai, F.; Kaji, D.; Kimura, S.; Morimoto, K.; Haba, H.; Jeong, S.; Koura, H.; et al. Status of the low-energy super-heavy element facility at RIKEN. *Nucl. Instrum. Methods Phys. Res. B* **2016**, *376*, 425–428. [CrossRef]
11. Cooper, K.; Sumithrarachchi, C.S.; Morrissey, D.J.; Levand, A.; Rodriguez, J.A.; Savard, G.; Schwarz, S.; Zabransky, B. Extraction of thermalized projectile fragments from a large volume gas cell. *Nucl. Instrum. Methods Phys. Res. A* **2014**, *763*, 543–546. [CrossRef]
12. Schwarz, S.; Bollen, G.; Chouhan, S.; Das, J.J.; Green, M.; Magsig, C.; Morrissey, D.J.; Ottarson, J.; Sumithrarachchi, C.; Villari, A.C.C.; et al. The NSCL cyclotron gas stopper—Entering commissioning. *Nucl. Instrum. Methods Phys. Res. B* **2016**, *376*, 256–259. [CrossRef]

13. Constantin, P.; Balabanski, D.L.; Anh, L.T.; Cuong, P.V.; May, B. Design of the gas cell for the IGISOL facility at ELI-NP. *Nucl. Instrum. Methods Phys. Res. B* **2017**, *397*, 1–10. [CrossRef]
14. Savard, G.; Levand, A.F.; Zabransky, B.J. The CARIBU gas catcher. *Nucl. Instrum. Methods Phys. Res. A* **2012**, *685*, 70–77. [CrossRef]
15. Saastamoinen, A.; Moore, I.D.; Ranjan, M.; Dendooven, P.; Penttilä, H.; Peräjärvi, K.; Popov, A.; Äystö, J. Characterization of a cryogenic ion guide at IGISOL. *Nucl. Instrum. Methods Phys. Res. B* **2016**, *376*, 246. [CrossRef]
16. Ranjan, M.; Dendooven, P.; Purushothaman, S.; Dickel, T.; Reiter, M.P.; Ayet, S.; Haettner, E.; Moore, I.D.; Kalantar-Nayestanaki, N.; Geissel, H.; et al. Design, construction and cooling system performance of a prototype cryogenic stopping cell for the super-FRS at FAIR. *Nucl. Instrum. Methods Phys. Res. A* **2015**, *770*, 87–97. [CrossRef]
17. Varentsov, V.; Yakushev, A. Concept of a new Universal High-Density Gas Stopping Cell Setup for study of gas-phase chemistry and nuclear properties of Super Heavy Elements (UniCell). *Nucl. Instrum. Methods Phys. Res. A* **2019**, *940*, 206–214. [CrossRef]
18. Varentsov, V.L.; Wada, M. Computer experiments on ion beam cooling and guiding in fair-wind gas cell and extraction RF-funnel system. *Nucl. Instrum. Methods Phys. Res. A* **2004**, *532*, 210. [CrossRef]
19. Varentsov, V.; Yakushev, A. Fair-wind gas cell for the UniCell setup. *Nucl. Instrum. Methods Phys. Res. A* **2021**, *1010*, 165487. [CrossRef]
20. Boussaid, R.; Ban, G.; Quéméner, G.; Merrer, Y.; Lorry, J. Development of a radio-frequency quadrupole cooler for high beam currents. *Phys. Rev. Accel. Beams* **2017**, *20*, 124701. [CrossRef]
21. Barquest, B.R.; Bollen, G.; Mantica, P.F.; Minamisono, K.; Ringle, R.; Schwarz, S. RFQ beam cooler and buncher for collinear laser spectroscopy of rare isotopes. *Nucl. Instrum. Methods Phys. Res. A* **2017**, *866*, 18–28. [CrossRef]
22. Schwarz, S.; Bollen, G.; Ringle, R.; Savory, J.; Schury, P. The LEBIT ion cooler and buncher. *Nucl. Instrum. Methods Phys. Res. A* **2017**, *816*, 131–141. [CrossRef]
23. Franberg, H.; Delahaye, P.; Billowes, J.; Blaum, K.; Catherall, R.; Duval, F.; Gianfrancesco, O.; Giles, T.; Jokinen, A.; Lindroos, M.; et al. Off-line commissioning of the ISOLDE cooler. *Nucl. Instrum. Methods Phys. Res. A* **2008**, *266*, 4502–4504. [CrossRef]
24. Barquest, B.R.; Bale, J.C.; Dilling, J.; Gwinner, G.; Kanungo, R.; Krücke, R.; Pearson, M.R. Development of a new RFQ beam cooler and buncher for the CANREB project at TRIUMF. *Nucl. Instrum. Methods Phys. Res. B* **2016**, *376*, 207–210. [CrossRef]
25. Brunner, T.; Smith, M.J.; Brodeur, M.; Ettenauer, S.; Gallant, A.T.; Simon, V.V.; Chaudhuri, A.; Lapierre, A.; Mane, E.; Ringle, R.; et al. TITAN's digital RFQ ion beam cooler and buncher, operation and performance. *Nucl. Instrum. Methods Phys. Res. A* **2012**, *676*, 32–43. [CrossRef]
26. Herfurth, F.; Dilling, J.; Kellerbauer, A.; Bollen, G.; Henry, S.; Kluge, H.-J.; Lamour, E.; Lunney, D.; Moore, R.B.; Scheidenberger, C.; et al. A linear radiofrequency ion trap for accumulation, bunching, and emittance improvement of radioactive ion beams. *Nucl. Instrum. Methods Phys. Res. A* **2001**, *469*, 254–275. [CrossRef]
27. Varentsov, V. *Review of Gas Dynamic RF-Only Funnel Technique for Ion Beams Cooling and Extraction into Vacuum*; FAIR: Darmstadt, Germany, 2022. [CrossRef]
28. Yanga, X.F.; Wang, S.J.; Wilkins, S.G.; Ruiz, R.F.G. Laser Spectroscopy for the Study of Exotic Nuclei. *Prog. Part. Nucl. Phys.* **2023**, *129*, 104005. [CrossRef]
29. Block, M.; Giacoppo, F.; Heßberger, F.-P.; Raeder, S. Recent progress in experiments on the heaviest nuclides at SHIP. *Riv. Nuovo Cim.* **2022**, *45*, 279–323. [CrossRef]
30. Van Duppen, P. In-Gas Jet Laser Ionization Spectroscopy of Heavy Elements. Available online: https://www.psi.ch/sites/default/files/import/ltp/ThursdayColloquiaEN/2018_11_Laser_spectroscopy_Heavy_Elements_Piet_Van_Duppen.pdf (accessed on 23 May 2023).
31. Kudryavtsev, Y.; Ferrer, R.; Huyse, M.; Van den Bergh, P.; Van Duppen, P. The in-gas-jet laser ion source: Resonance ionization spectroscopy of radioactive atoms in supersonic gas jets. *Nucl. Instrum. Methods Phys. Res. B* **2013**, *297*, 7–22. [CrossRef]
32. Raeder, S.; Block, M.; Chhetri, P.; Ferrer, R.; Kraemer, S.; Kron, T.; Laatiaoui, M.; Nothhelfer, S.; Schneider, F.; Van Duppen, P.; et al. A gas-jet apparatus for high-resolution laser spectroscopy on the heaviest elements at SHIP. *Nucl. Instrum. Methods Phys. Res. B* **2020**, *463*, 272–276. [CrossRef]
33. Münzberg, D.; Block, M.; Claessens, A.; Ferrer, R.; Laatiaoui, M.; Lantis, J.; Nothhelfer, S.; Raeder, S.; Van Duppen, P. Resolution Characterizations of JetRIS in Mainz Using ^{164}Dy. *Atoms* **2022**, *10*, 57. [CrossRef]
34. Ferrer, R.; Barzakh, A.; Bastin, B.; Beerwerth, R.; Block, M.; Creemers, P.; Grawe, H.; de Groote, R.; Delahaye, P.; Fle, X.; et al. Towards high-resolution laser ionization spectroscopy of the heaviest elements in supersonic gas jet expansion. *Nat. Commun.* **2017**, *8*, 14520. [CrossRef] [PubMed]
35. Ferrer, R.; Verlinde, M.; Verstraelen, E.; Claessens, A.; Huyse, M.; Kraemer, S.; Kudryavtsev, Y.; Romans, J.; Van den Bergh, P.; Van Duppen, P.; et al. Hypersonic nozzle for laser-spectroscopy studies at 17 K characterized by resonance-ionization-spectroscopy-based flow mapping. *Phys. Rev. Res.* **2021**, *3*, 043041. [CrossRef]
36. Sels, S.; Ferrer, R.; Dockx, K.; Buitrago, C.G.; Huyse, M.; Kudryavtsev, Y.; Kraemer, S.; Raedera, S.; Van Den Bergh, P.; Van Duppen, P.; et al. Design and commissioning of an ion guide system for In-Gas Laser Ionization and Spectroscopy experiments. *Nucl. Instrum. Methods Phys. Res. B* **2020**, *463*, 148–153. [CrossRef]
37. Romans, J.; Ajayakumar, A.; Authier, M.; Boumard, F.; Caceres, L.; Cam, J.-F.; Claessens, A.; Damoy, S.; Delahaye, P.; Desrues, P.; et al. First Offline Results from the S^3 Low-Energy Branch. *Atoms* **2022**, *10*, 21. [CrossRef]
38. Hirayama, Y.; Watanabe, Y.X.; Schury, P.; Mukai, M.; Choi, H.; Ahmed, M.; Kakiguchi, Y.; Oyaizu, M.; Wada, M.; Miyatake, H. In-gas-jet laser ionization spectroscopy at KISS. *RIKEN Accel. Prog. Rep.* **2019**, *52*, 1.

39. Varentsov, V.L.; Ignatiev, A.A. Numerical investigations of internal supersonic jet targets formation for storage rings. *Nucl. Instrum. Methods Phys. Res. A* **1998**, *413*, 447–456. [CrossRef]
40. Varentsov, V.L. Focused ion beam source of a new type for micro- and nanoelectronic technologies. In *Micro- and Nanoelectronics*; SPIE: Philadelphia, PA, USA, 2008; Volume 7025, pp. 702509–702521. [CrossRef]
41. Varentsov, V. Proposal of an RF-Only Double-Funnel System for Ions Extraction from a Cryogenic Stopping Cell for the Super-FRS at FAIR. *GSI Sci. Rep.* **2015**, *1*, 503–504. [CrossRef]
42. Varentsov, V. Proposal of a new Laser ablation ion source for LaSpec and MATS testing. In Proceedings of the NUSTAR Collaboration Meeting, Darmstadt, Germany, 29 February–4 March 2016. [CrossRef]
43. Brunner, T.; Fudenberg, D.; Varentsov, V.; Sabourov, A.; Gratta, G.; Dilling, J.; nEXO Collaboration. An RF-only ion-funnel for extraction from high-pressure gases. *Int. J. Mass Spectrom.* **2015**, *379*, 110–120. [CrossRef]
44. Ratajczyk, T.; Bollinger, P.; Lellinger, T.; Varentsov, V.; Nörtershäuser, W. Towards a He-buffered laser ablation ion source for collinear laser spectroscopy. *Hyperfine Interact* **2020**, *241*, 52. [CrossRef]
45. Valverde, A.A.; Brodeur, M.; Burdette, D.P.; Clark, J.A.; Klimes, J.W.; Lascar, D.; O'Malley, P.D.; Ringle, R.; Savard, G.; Varentsov, V. Stopped, bunched beams for the twinsol facility. *Hyperfine Interact* **2019**, *240*, 38. [CrossRef]
46. O'Malley, P.D.; Brodeur, M.; Burdette, D.P.; Klimes, J.W.; Valverde, A.; Clark, J.A.; Savard, G.; Ringle, R.; Varentsov, V. Testing the weak interaction using St. Benedict at the University of Notre Dame. *Nucl. Instrum. Methods Phys. Res. B* **2020**, *463*, 488–490. [CrossRef]
47. Murray, K.; Dilling, J.; Gornea, R.; Ito, Y.; Koffas, T.; Kwiatkowski, A.A.; Lan, Y.; Reiter, M.P.; Varentsov, V.; Brunner, T. With the nEXO collaboration. Design of a Multiple-Reflection time-of-flight Mass-Spectrometer for Barium-tagging. *Hyperfine Interact* **2019**, *240*, 97. [CrossRef]
48. Querci, L.; Varentsov, V.; Günther, D.; Hattendorf, B. An RF-only ion funnel interface for ion cooling in laser ablation time of flight mass spectrometry. *Spectrochim. Acta B* **2018**, *146*, 57–68. [CrossRef]
49. Tiedemann, D.; Stiebing, K.E.; Winters, D.F.A.; Quint, W.; Varentsov, V.; Warczak, A.; Malarz, A.; Stöhlker, T. A pulsed supersonic gas jet target for precision spectroscopy at the HITRAP facility at GSI. *Nucl. Instrum. Methods Phys. Res. A* **2014**, *764*, 387–393. [CrossRef]
50. Varentsov, V.L.; Kuroda, N.; Nagata, Y.; Torii, H.A.; Shibata, M.; Yamazaki, Y. ASACUSA Gas-Jet Target: Present Status and Future Development. *AIP Conf. Proc.* **2005**, *793*, 328–340. [CrossRef]
51. Yakushev, A.; Wey, Y.; Simonovski, D.; Düllmann, C.E.; Vrentsov, V. Towards chemistry beyond moscovium (Mc, Z = 115). In Proceedings of the TASCA Collaboration Meeting, Rennes, France, 9–11 May 2022. [CrossRef]
52. Varentsov, V.L.; Yaschuk, V.V. Technique of Phase Volume Decrease of an Atomic Beam. Inventor's Certificate (USSR) Patent No. 774523, 14 May 1979.
53. Varentsov, V.L.; Yashchuk, V.V. Gasdynamic method for reducing the phase volume of an atomic beam. *Sov. Tech. Phys. Lett.* **1983**, *9*, 65–66.
54. Varentsov, V.L. The Method of an Atomic Beam Phase Volume Decrease and Its Possible Application for Atomic and Nuclear Physics Problems. Ph.D. Thesis, Leningrad Nuclear Physics Institute, Gatchina, Russia, 1986; pp. 1–140. (In Russian).
55. Varentsov, V.L. Gas dynamic cooling of low-energy molecular and ion beams. *J. Technol. Phys.* **1994**, *39*, 358–363.
56. Varentsov, V.L.; Ezhov, V.F.; Kniaz'kov, V.A.; Ryabov, V.L.; Khazov, A.Y.; Yaschuk, V.V. Time-of-flight molecular-beam spectrometer. *Prib. Tekh. Eksp.* **1986**, *1*, 152–154.
57. Varentsov, V.L.; Ezhov, V.F.; Kniaz, V.A.; Muratov, V.G.; Ryabov, V.L.; Khazov, A.Y.; Yaschuk, V.V. High-intensity gas dynamic molecular beam source of a new type. *J. Tech. Phys.* **1987**, *57*, 755.
58. Varentsov, V.L.; Hansevarov, D.R. A new approach to the nozzle design of gas-jet targets. *Nucl. Instrum. Methods Phys. Res. A* **1992**, *317*, 1–6. [CrossRef]
59. Varentsov, V.L.; Hansevarov, D.R.; Varentsov, D.V. The generation of an internal molecular-beam target from expensive gaseous and nonvolatile substances for storage rings. *Nucl. Instrum. Methods Phys. Res. A* **1995**, *352*, 542–547. [CrossRef]
60. Varentsov, V. Windowless gas dynamic ion beam cooler and buncher. *Nucl. Instrum. Methods Phys. Res. A* **2020**, *984*, 164596. [CrossRef]
61. Varentsov, V. *Gas Dynamic Cooling of Low Energy Molecular and Ion Beams*; Stefan Meyer Institute (SMI)): Vienna, Austria, 2004. [CrossRef]